



UNIVERSITY OF LEEDS

This is a repository copy of *Linear and nonlinear dynamics of cylindrically and spherically expanding detonation waves*.

White Rose Research Online URL for this paper:  
<http://eprints.whiterose.ac.uk/7930/>

---

**Article:**

Watt, S.D. and Sharpe, G.J. (2005) Linear and nonlinear dynamics of cylindrically and spherically expanding detonation waves. *Journal of Fluid Mechanics*, 522. pp. 329-356.  
ISSN 0022-1120

<https://doi.org/10.1017/S0022112004001946>

---

**Reuse**

See Attached

**Takedown**

If you consider content in White Rose Research Online to be in breach of UK law, please notify us by emailing [eprints@whiterose.ac.uk](mailto:eprints@whiterose.ac.uk) including the URL of the record and the reason for the withdrawal request.



[eprints@whiterose.ac.uk](mailto:eprints@whiterose.ac.uk)  
<https://eprints.whiterose.ac.uk/>

# Linear and nonlinear dynamics of cylindrically and spherically expanding detonation waves

By SIMON D. WATT AND GARY J. SHARPE†

School of Mathematics and Statistics, University of Birmingham, Edgbaston,  
Birmingham B15 2TT, UK

(Received 27 October 2003 and in revised form 1 September 2004)

The nonlinear stability of cylindrically and spherically expanding detonation waves is investigated using numerical simulations for both directly (blast) initiated detonations and cases where the simulations are initialized by placing quasi-steady solutions corresponding to different initial shock radii onto the grid. First, high-resolution one-dimensional (axially or radially symmetric) simulations of pulsating detonations are performed. Emphasis is on comparing with the predictions of a recent one-dimensional linear stability analysis of weakly curved detonation waves. The simulations show that, in agreement with the linear analysis, increasing curvature has a rapid destabilizing effect on detonation waves. The initial size and growth rate of the pulsation amplitude decreases as the radius where the detonation first forms increases. The pulsations may reach a saturated nonlinear behaviour as the amplitude grows, such that the subsequent evolution is independent of the initial conditions. As the wave expands outwards towards higher (and hence more stable) radii, the nature of the saturated nonlinear dynamics evolves to that of more stable behaviour (e.g. the amplitude of the saturated nonlinear oscillation decreases, or for sufficiently unstable cases, the oscillations evolve from multi-mode to period-doubled to limit-cycle-type behaviour). For parameter regimes where the planar detonation is stable, the linear stability prediction of the neutrally stable curvature gives a good prediction of the location of the maximum amplitude (provided the stability boundary is reached before the oscillations saturate) and of the critical radius of formation above which no oscillations are seen. The linear analysis also predicts very well the dependence of the period on the radius, even in the saturated nonlinear regimes. Secondly, preliminary two-dimensional numerical simulations of expanding cellular detonations are performed, but it is shown that resolved and accurate calculations of the cellular dynamics are currently computationally prohibitive, even with a dynamically adaptive numerical scheme.

---

## 1. Introduction

Detonation waves are powerful and rapid (supersonic) combustion waves which can propagate through reactive materials. These waves consist of a shock wave, which raises the pressure and temperature of the explosive, initiating the chemical reactions, and an exothermic reaction zone, the heat release of which provides the energy to drive the wave forward. Detonations are prone (especially in gaseous mixtures) to both a pulsating instability in which the front oscillates longitudinally and a

† Present address: Los Alamos National Laboratory, New Mexico, NM 87545, USA.

multi-dimensional cellular instability in which the front becomes wrinkled (Fickett & Davis 1979). Predicting different instability regimes and understanding of these instabilities is important if one wishes to control detonation processes, either for applications which make use of the power of these waves, such as in Pulsed Detonation Engine technology, or for explosion safety issues (i.e. in preventing unplanned detonations).

The majority of previous theoretical work on detonation instabilities has concerned planar detonation waves, relevant to detonation waves in channels or square tubes. This includes linear stability analyses of steady, planar detonations (e.g. Short & Stewart 1998), weakly nonlinear theories (e.g. Short 2001), one-dimensional numerical simulations of pulsating detonations (e.g. Sharpe & Falle 2000a; Radulescu *et al.* 2002) and multi-dimensional simulations of cellular detonations (e.g. Sharpe 2001; Bourlioux & Majda 1992). However, if the detonation propagates through an unconfined reactive material (such as cylindrically or spherically expanding detonations initiated by a high-energy source, or detonation diffraction when the wave exits from the end of a tube) or the reactive material is weakly confined by a surrounding inert material (e.g. sticks of explosives or gaseous detonations propagating in porous walled tubes), then the wave front is globally curved. In these cases, it is important to understand how this global curvature affects the stability of the detonation and conversely how the instabilities affect the propagation of the curved detonation front.

Recently, Watt & Sharpe (2003) performed a one-dimensional linear stability analysis (corresponding to the pulsating detonation instability) of weakly curved, quasi-steady detonations. This analysis predicts that even weak curvature will have a significant destabilizing effect on detonations, as well as providing a prediction of neutral stability boundaries, i.e. critical curvatures above which the front becomes unstable. This appears to agree with one-dimensional numerical simulations of directly initiated radially expanding detonations (He & Clavin 1994; Eckett, Quirk & Shepherd 2000; Sharpe 2000; Ng & Lee 2003) which show that the curved detonation may be unstable even when the planar wave is stable, but that the expanding waves become less unstable as the radius of the front increases. However, these previous simulations of radially expanding detonations were mainly concerned with the direct initiation problem (i.e. with criteria for the minimum source energy required for initiating the detonation) or with the quasi-steady state, rather than with the nature of the nonlinear stability of the wave itself, and had no stability analysis with which to compare.

The main purpose of this paper is to compare nonlinear calculations with the predictions of the linear stability analysis in Watt & Sharpe (2003), and to investigate how curvature affects the nonlinear stability of detonation waves. Here we perform numerical simulations of cylindrically and spherically expanding detonation waves, since this is the simplest geometry in which curvature of detonation fronts is important. Indeed, this case is sufficiently simple that one-dimensional (axially or radially symmetric) simulations are possible, and hence we can compare directly with the one-dimensional stability analysis in Watt & Sharpe (2003). Such expanding detonations can be initiated by a sufficiently high-energy line or point source in cylindrical and spherical geometry, respectively. For example, a cylindrically expanding detonation in a reactive gas may be initiated by a length of exploding cord embedded in the gas (Radulescu *et al.* 2003), while small spherical sources of solid explosives have been used to initiate spherical detonations (Radulescu *et al.* 2000). However, it should be stressed that while in our simulations the radially expanding detonations are initiated by high-energy line or point sources, we are not concerned with the direct initiation problem itself, but with the nonlinear dynamics of the propagation of the detonation wave after it has formed.

The plan of the paper is as follows: the mathematical model is described in §2; quasi-steady solutions to these equations and their linear stability are reviewed in §3; the numerical method is described in §4; the results for the pulsating and cellular instabilities are given in §5 and §6, respectively; §7 contains the conclusions and ideas for future work.

## 2. Governing equations

In this paper we use the standard, idealized model of a detonation with a single, irreversible reaction,  $A \rightarrow B$ . This is the model used in the stability analysis of Watt & Sharpe (2003) with which we wish to compare. In one dimension the governing equations are thus

$$\frac{\partial \rho}{\partial t} + \frac{\partial(\rho u)}{\partial r} + \frac{j}{r}(\rho u) = 0, \quad (2.1)$$

$$\frac{\partial(\rho u)}{\partial t} + \frac{\partial(\rho u^2 + p)}{\partial r} + \frac{j}{r}(\rho u^2) = 0, \quad (2.2)$$

$$\frac{\partial(\rho e)}{\partial t} + \frac{\partial(\rho u e + p u)}{\partial r} + \frac{j}{r}(\rho u e + p u) = 0, \quad (2.3)$$

$$\frac{\partial(\rho \lambda)}{\partial t} + \frac{\partial(\rho u \lambda)}{\partial r} + \frac{j}{r}(\rho u \lambda) = -\alpha \lambda \exp(-\tau/T) = W, \quad (2.4)$$

where  $\rho$  is the density of the fluid,  $u$  the velocity,  $p$  the pressure,

$$e = \frac{p}{(\gamma - 1)\rho} + \frac{1}{2}u^2 - q(1 - \lambda)$$

the total energy per unit mass,  $\lambda$  the reaction progress variable or fuel mass fraction (with  $\lambda = 1$  for completely unburnt and  $\lambda = 0$  for completely burnt),  $T = p/\rho$  is the temperature,  $\alpha$  the rate constant,  $\tau$  the activation temperature,  $\gamma$  the (constant) ratio of specific heats,  $q$  the heat of reaction and  $j = 1$  for cylindrical geometry or  $j = 2$  for spherical geometry. Equations (2.1)–(2.4) have been non-dimensionalized using the upstream density and the speed and half-reaction length of the steady planar Chapman–Jouguet (CJ) (self-supporting) detonation (these scalings are described more fully in Sharpe 1997). However, for detonation stability studies, the activation temperature and heat of reaction are usually given in terms of Erpenbeck's (1964) scalings for these parameters,  $E$  and  $Q$  (i.e. those scaled with the upstream temperature). Here we will set  $Q = 50$  and  $\gamma = 1.2$  and vary the activation temperature ( $E$ ). The relationship between the scalings is  $\tau = p_0 E$  and  $q = p_0 Q$  where  $p_0$  is the dimensionless upstream pressure in our scalings, with  $p_0 = 0.0216$  for  $Q = 50$  (Sharpe 1997).

## 3. Quasi-steady solutions and linear stability

For a stable radially expanding detonation, numerical simulations of the reactive Euler equations show that the instantaneous speed and structure of the detonation at a given shock radius are described accurately by a quasi-steady analysis (Sharpe 2000; Short & Sharpe 2003), i.e. the assumption that the front evolves on a timescale which is long compared to the particle transit time through the reaction zone holds. Stable expanding detonation fronts are therefore described to leading order by the quasi-steady version of equations (2.1)–(2.4), which, written in a frame attached to

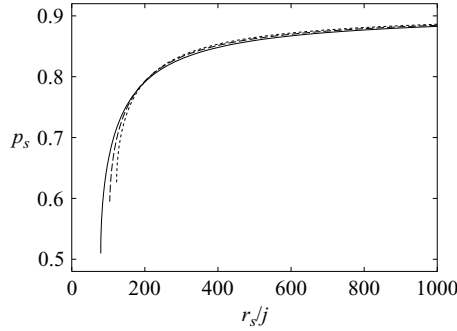


FIGURE 1. The quasi-steady shock pressure–shock radius relation for  $E = 20$  (solid line),  $E = 24$  (dashed line) and  $E = 27$  (dotted line).

the shock, are

$$\left. \begin{aligned} \frac{d(\rho u_n)}{dn} + \frac{j}{r_s} \rho (u_n + D_n) &= 0, & u_n \frac{du_n}{dn} + \frac{1}{\rho} \frac{dp}{dn} &= 0, & \frac{de}{dn} - \frac{p}{\rho^2} \frac{d\rho}{dn} &= 0, \\ u_n \frac{d\lambda}{dn} + \alpha \lambda \exp(-\tau/T) &= 0 \end{aligned} \right\} \quad (3.1)$$

(see, for example, He & Clavin 1994 or Yao & Stewart 1996), accurate to  $O(1/r_s)$ . Here  $n$  is now the radial distance behind the shock,  $u_n$  is the radial gas velocity as measured in the instantaneous shock rest frame,  $D_n$  is the instantaneous shock velocity and  $r_s$  is the shock radius, such that  $\kappa = j/r_s$  is the curvature of the front.

Equations (3.1), together with the shock jump conditions at  $n = 0$  and a generalized CJ (sonic) condition near the rear of the reaction zone, lead to an eigenvalue problem for determining the detonation speed  $D_n$  (or equivalently the shock pressure,  $p_s$ , which is related to  $D_n$  via the shock jump conditions by  $D_n^2 = \gamma p_0 [(p_s/p_0 - 1)(\gamma + 1)/(2\gamma + 1)]$ ) for a given radius of curvature of the front,  $r_s$  (e.g. He & Clavin 1994; Yao & Stewart 1996). The numerical shooting method that we employ for solving this eigenvalue problem is described in Watt & Sharpe (2003). Figure 1 shows the eigenvalue relationship between the shock pressure and shock radius (the quasi-steady  $p_s$ – $r_s$  curves), as determined from this quasi-steady analysis, for several activation temperatures. Points to note are that (i) the shock pressure increases as the wave expands outwards, and approaches the planar value (0.907 in our scalings) as the curvature tends to zero, (ii) there exists a critical radius of curvature below which there is no quasi-steady solution, and hence detonations cannot propagate in a quasi-steady fashion below the corresponding critical shock radius. Note also that the critical radius increases (critical curvature decreases) as the activation temperature increases.

However, for expanding detonation fronts one needs to check the quasi-steady solution for self-consistency. One of the time-dependent terms neglected in the approximations leading to equations (3.1) is the shock acceleration term,  $\dot{D}_n$  (in the momentum equation, see Yao & Stewart 1996). Given the quasi-steady  $D_n$ – $r_s$  relation the acceleration term is then  $\dot{D}_n = \dot{r}_s dD_n/dr_s = D_n dD_n/dr_s$ , which becomes infinite at the critical shock radius turning point. Hence the quasi-steady assumption must break down as the critical shock radius is approached, i.e. time-dependence must be reinstated near this point and the quasi-steady solution cannot represent the underlying wave here.

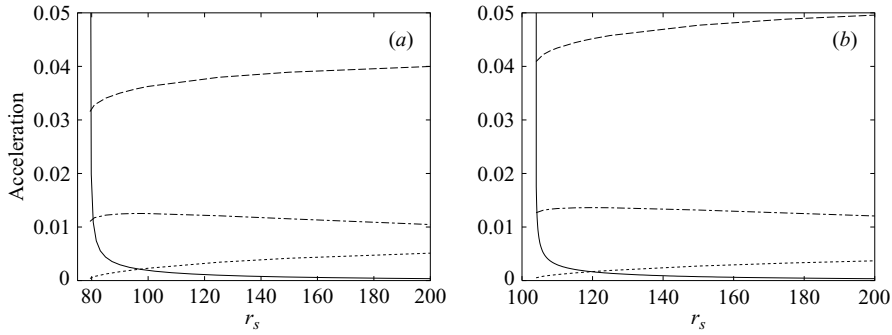


FIGURE 2. Quasi-steady acceleration  $\dot{D}_n$  (solid lines), and maximum, minimum and sonic values of the magnitude of  $u_n du_n/dn$  in the quasi-steady wave (dashed, dotted and dot-dashed lines respectively) against shock radius for the cylindrical case, for (a)  $E = 20$  and (b)  $E = 24$ .

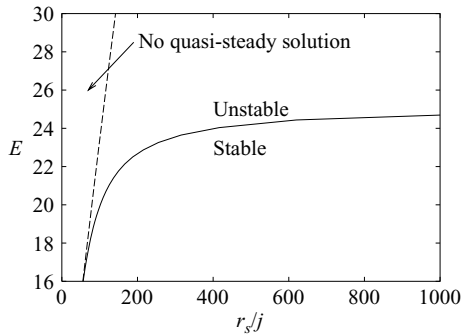


FIGURE 3. The neutral stability boundary from the linear stability analysis in Watt & Sharpe (2003). Also shown is the critical radius of curvature for the quasi-steady solutions (dashed line).

In order to estimate how close to the critical radius the quasi-steady approximation breaks down, we here compare the size of the shock acceleration term neglected in the momentum equation to that of the non-neglected fluid acceleration term,  $u_n du_n/dn (= -\rho^{-1} dp/dn)$  in the quasi-steady solution. Figure 2 shows  $\dot{D}_n$  and the maximum, minimum and sonic-point magnitude of  $u_n du_n/dn$ , against  $r_s$  according to the quasi-steady solution, for the cylindrical cases with  $E = 20$  and  $E = 24$ . Note that the minimum of  $u_n du_n/dn$  occurs at the shock. The most important point is that the time-dependent terms must be negligible at the sonic point, in order that they do not significantly disrupt the delicate balance between curvature and thermicity there. However, we will take the more stringent condition that  $\dot{D}_n$  is negligible everywhere in the quasi-steady reaction zone for the quasi-steady approximation to be self-consistent. Figure 2 shows that the shock acceleration becomes smaller than the value of  $u_n du_n/dn$  at the shock at  $r_s = 97.0$  for  $E = 20$  and  $r_s = 119.7$  for  $E = 24$  (while for  $E = 27$  this occurs at  $r_s = 139.9$ ). Hence for the cases we consider in this paper, the quasi-steady solution should be a good approximation to the underlying wave for shock radii above distances of  $\sim 20$  from the critical shock radius.

As a first step towards understanding the effects of curvature on the stability of detonation waves, Watt & Sharpe (2003) investigated the leading-order linear stability response of the underlying quasi-steady waves described above. Figure 3 shows the

neutral stability boundary accurate to  $O(1/r_s)$  as determined by this linear stability analysis in an activation temperature–shock radius diagram. Also shown in figure 3 is the locus of the critical radius of curvature, below which there are no quasi-steady solutions. The main result in Watt & Sharpe (2003), apart from the determination of the neutral stability curves, is that the linear stability analysis shows that even a small increase in curvature has a rapid destabilizing effect on detonation waves. Indeed, as can be seen from figure 3, even if the planar ( $r_s = \infty$ ) wave is stable for fixed activation temperature, the front always becomes unstable for sufficiently low shock radius. Note that the neutral stability boundary in figure 3 asymptotes to the quasi-steady critical shock radius locus, so that the detonation is always unstable sufficiently near the critical curvature, even for quite low activation temperatures. However, note that since the underlying quasi-steady approximation must break down sufficiently near the critical curvature for expanding detonations, the neutral stability boundary becomes meaningless for low enough  $E$  (below about  $E = 20$  according to the above estimates of the region of self-consistency of the quasi-steady assumption). One of the main purposes of this paper is to compare the linear stability predictions with the fully nonlinear numerical simulations for various activation temperatures (with  $E \geq 20$ ).

#### 4. Numerical method

In order to perform the numerical simulations we used the dynamically adaptive industrial code  $\mu$ Cobra, which is fully described in Sharpe & Falle (2000*b*, and references contained therein). This code uses a second-order Godunov-type scheme and a hierarchical series of grids  $G^0, \dots, G^N$ , so that grid  $G^n$  has mesh spacing  $h/2^n$ , where  $h$  is the mesh spacing on the base grid  $G^0$ . Grids  $G^0$  and  $G^1$  cover the whole domain, but the higher grids only occupy regions where increased resolution is required. The code automatically refines shocks onto the highest grid level, and the reaction zone of the detonation is also fully refined to level  $G^N$  by forcing refinement whenever  $\lambda > 0.1$  or  $|W| > 0.01$  (where  $W$  is the reaction rate) behind the shock.

For the one-dimensional calculations in §5, we use a base grid spacing of 1 point per unit  $r$  and seven refinement levels, giving an effective resolution of 128 grid points per half-reaction length (points/ $l_{1/2}$ ) of the steady, planar detonation, which is sufficient to give well-converged results for the nonlinear instability (Sharpe & Falle 2000*a*). The boundary conditions are a symmetry condition at  $r=0$  and a free-flow (zero-gradient) condition at the other boundary (located at a value of  $r$  which is typically a few thousand). For the most part, we give results for cylindrical geometry since the main results and conclusions are similar for both geometries.

We initialize the simulations in two ways. First, we consider the initial value problem of directly initiated detonations. For this case the initial conditions are given by  $\rho = 1$ ,  $u = 0$  and  $\lambda = 1$  everywhere, with a high-energy source at the origin given by a ‘top hat’ profile for the pressure with  $p = 0.0216$  (the upstream pressure corresponding to  $Q = 50$ ) for  $r > r_{\text{source}}$  and  $p = p_{\text{source}}$  for  $r \leq r_{\text{source}}$ . The source (initiation) energy, i.e. the energy in the high-pressure region, is hence given by

$$E_{\text{source}} = \begin{cases} \frac{\pi(r_{\text{source}})^2 p_{\text{source}}}{(\gamma - 1)}, & \text{cylindrical geometry (line source)} \\ \frac{4\pi(r_{\text{source}})^3 p_{\text{source}}}{3(\gamma - 1)}, & \text{spherical geometry (point source)}. \end{cases}$$

One half-reaction length is typically used for the hot-spot radius,  $r_{\text{source}} = 1$ . This initial condition quickly produces a classical self-similar strong blast wave. Provided the source energy is sufficiently high then as the blast wave expands outwards and decays, the shock and exothermicity of the reactions begin to couple and eventually produce a radially expanding detonation (see Ng & Lee 2003). For convenience we define a scaled source energy by

$$E_s = \begin{cases} (\gamma - 1)E_{\text{source}}/\pi & \text{(cylindrical geometry)} \\ 3(\gamma - 1)E_{\text{source}}/4\pi & \text{(spherical geometry)}. \end{cases}$$

While this initial value problem is more physically realistic and allows us to investigate the complete nonlinear evolution from initiation onwards, this is not a clean problem for comparing directly with the linear stability analysis of the quasi-steady solutions, because the stability and initiation characteristics may overlap, i.e. for cases where the blast wave approaches the quasi-steady curve near the critical shock radius it is difficult to assess where the underlying wave would have become quasi-steady (if it were stable) and thus to ensure that the pulsations belong to a fully formed detonation. Hence in order to compare the nonlinear results more directly with the linear stability predictions, we also consider cases where we initialize the simulations by placing the quasi-steady solution (obtained by numerical integration of equations (3.1)) corresponding to various values of  $r_s$  onto the numerical grid. In this case the perturbation to the quasi-steady solution is mainly due to the startup error from the initial smearing out of the shock, as usual (see Sharpe & Falle 2000*a*, for example).

For the two-dimensional simulations of cylindrically expanding fronts in §6, Cartesian coordinates are used, with the numerical domain consisting of the quarter-plane  $x \geq 0$ ,  $y \geq 0$ , with symmetry boundary conditions at  $x = 0$  and  $y = 0$  (and free-flow conditions at the other two boundaries). The initial conditions are similar to those of the one-dimensional simulations (i.e. a high pressure in the region  $x^2 + y^2 \leq (r_{\text{source}})^2$ ).

## 5. Pulsating instability

In this section we give the results of the one-dimensional simulations for various activation temperatures and source energies. In discussing these results, it is instructive to review the one-dimensional nonlinear stability of planar detonation fronts described in Sharpe & Falle (2000*a*). First, for planar waves, when the initial conditions are given by the underlying steady detonation, the linear stability analysis accurately predicts the stability boundaries as a stability parameter (e.g. the activation temperature) is varied. For unstable cases there are two stages in the evolution. Initially the shock speed (or pressure) begins to oscillate with an exponentially growing amplitude. As the stability parameter is varied such that the linear analysis predicts that the steady wave becomes more unstable, the initial growth rate of the oscillations increases as expected.

However, the amplitude of the oscillations eventually saturates as it reaches a nonlinear equilibrium behaviour. Sufficiently near the stability boundary this saturated nonlinear behaviour is that of a limit cycle (constant-amplitude oscillations). The final amplitude of the limit-cycle oscillation is smaller for less unstable values of the stability parameter. However, one important point to note is that as the neutrally stable value of the parameter is approached, the limit cycle amplitude does not tend

to zero (although the linear growth rate of the initial stage does). Hence for very weakly unstable cases the oscillations grow very slowly, but still eventually saturate at some finite amplitude. Further from the stability boundary the saturated nonlinear behaviour undergoes period doubling bifurcations, and for sufficiently unstable waves, the final behaviour may be multi-mode or chaotic.

The main difference between the previous one-dimensional simulations of planar detonations and those for radially expanding detonations considered here, is that our main stability parameter (the curvature of the front) is not a constant but changes in time (towards more stable values according to the linear stability analysis in Watt & Sharpe 2003) as the wave front expands outwards. Hence we may expect the initial growth rate to depend on the radius at which the detonation first forms, and, once reached, for the saturated nonlinear behaviour to also evolve in time.

### 5.1. $E = 20$

For an activation temperature of  $E = 20$ , the planar wave is highly stable, and the linear stability analysis in Watt & Sharpe (2003) predicts that the radius of curvature has to be sufficiently near the critical quasi-steady radius for the front to be one-dimensionally unstable (the linear analysis predicts the neutrally stable radius to be at  $r_s/j = 104$ , compared to the critical quasi-steady radius of  $r_s/j = 79.4$ ). Since the quasi-steady solution is predicted to be stable away from the critical radius, this is an instructive case to consider in order to explore the dependence of the radius of formation of the quasi-steady detonation on the source energy, and also for separating aspects of the initiation process from the stability issue.

One important point to note is that, in planar geometry, Mazaheri (1997) and Sharpe & Falle (2000a) have shown that a drawback of the standard one-step reaction model used here is that it has no definite detonability limit, and hence, unrealistically, a detonation will always be generated after a sufficiently long time, so that a critical source energy cannot be properly defined. However, for cylindrical or spherical waves it appears that the additional geometric expansion behind the shock is sufficient to produce a definite critical source energy even for the one-step model, or at least a sharp distinction between source energies producing a prompt initiation of the detonation and those for which no detonation is initiated for exponentially long times (Eckett *et al.* 2000). Nevertheless, as pointed out by Ng & Lee (2003), if one is mainly concerned with the direct initiation problem, a more realistic chemical model with an intrinsic chemically based detonability limit should be employed.

Figure 4(a) shows the shock pressure as a function of shock radius in the cylindrical case for source energies very near the critical value (below which the shock pressure drops to low values for a exponentially long period of time during which no detonation is initiated). In this case the critical source energy is  $E_s = 572.4$ . Just above the critical value, the blast wave pressure drops to low values before an ignition process, which starts behind the shock, overtakes the front, resulting in the formation of a highly overdriven detonation that then decays towards the quasi-steady state (see Ng & Lee 2003 and Mazaheri 1997 for an explanation of the mechanisms of this process). Note that once the detonation has become self-sustaining, it follows the quasi-steady  $p_s-r_s$  curve. Note also that as the critical source energy is approached from above, the radius at which the ignition event occurs (and the radius where the subsequently produced detonation becomes self-sustaining) increases, as well as becoming more and more sensitive to the value of  $E_s$ . Finally, note that for the critical source energy in such stable cases, the decaying blast wave cuts the quasi-steady  $p_s-r_s$  curve very close to the turning point of this curve (cf. He & Clavin 1994; Short & Sharpe 2004).

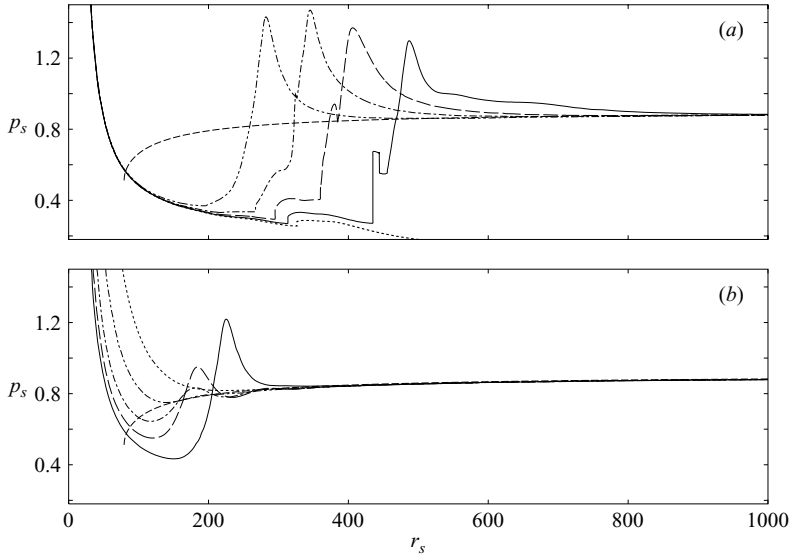


FIGURE 4. Shock pressure versus shock radius in cylindrical geometry for  $E = 20$  and (a)  $E_s = 572.3$  (dotted line), 572.4 (solid line), 573 (long-dashed line), 574 (dot-dashed line) and 580 (double-dot-dashed line), and (b)  $E_s = 600$  (solid line), 700 (long-dashed line), 900 (dot-dashed line), 1500 (double-dot dashed line) and 3000 (dotted line). The short-dashed curve is the quasi-steady  $p_s-r_s$  relation.

One should be careful in distinguishing the pulse in the pressure history produced by the ignition process from anything to do with the pulsating instability of the detonation, since a propagating detonation has not formed until after this ignition process has taken place. Indeed, the evolution for sufficiently supercritical source energies shows that the underlying quasi-steady state is stable at the radii where the ignition takes place in these near critical cases (see figure 4b), in agreement with the prediction of the linear stability analysis. Hence for the more unstable cases considered below, we will call this first pulse the ‘ignition pulse’ to distinguish it from the pulsations due to the instability of the propagating detonation which is subsequently formed. As we will see, it is the radius where the detonation approaches the quasi-steady state after the ignition pulse which determines the subsequent stability of the detonation, rather than the radius where the blast wave pressure first intersects the quasi-steady  $p_s-r_s$  curve.

Figure 4(b) shows the shock pressure evolution for increasingly supercritical source energies. As  $E_s$  continues to increase away from the critical value, the ignition pulse and subsequent quasi-steady detonation formation occur at smaller radii, and the amplitude of the ignition pulse decreases. However, for sufficiently supercritical values, the blast wave decays smoothly until it reaches the quasi-steady  $p_s-r_s$  curve and subsequently follows closely the quasi-steady solution. Hence in this final regime the blast wave pressure never drops below the quasi-steady shock pressure, and as  $E_s$  is increased further the shock decays towards the quasi-steady state at a larger radius, and thus the detonation forms at larger  $r_s$ .

In summary, the main result determined from this stable case is that as the source energy increases from its critical value, the radius where the detonation forms initially decreases, until a particular value of source energy is reached,  $E_s^*$ , say. For  $E_s > E_s^*$ , the radius of detonation formation begins to increase. Hence there is a minimum

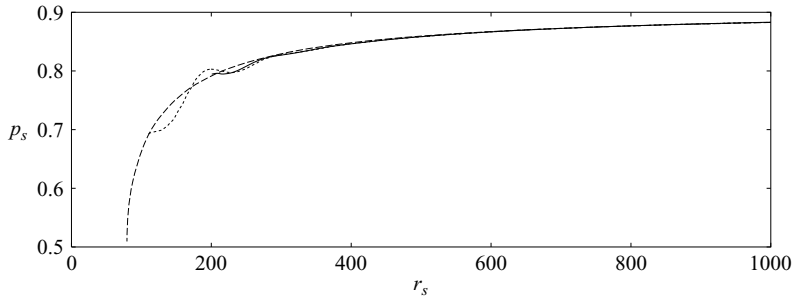


FIGURE 5. Shock pressure versus shock radius in cylindrical geometry for  $E = 20$  when the simulations are initialized by the quasi-steady solutions corresponding to  $r_s = 110$  (dotted line) and 200 (solid line). The dashed curve is the quasi-steady  $p_s$ - $r_s$  relation.

formation radius corresponding to  $E_s^*$ . For example, for  $E = 20$  figure 4 shows that  $E_s^* \sim 1500$ . Since the linear stability analysis predicts that, for fixed higher activation temperatures, the detonation will be more unstable at smaller shock radii of curvature, we therefore expect that the most unstable initial behaviour of the detonation (e.g. most rapid growth rate of the pulsations) will be seen for source energies close to  $E_s^*$ , with the detonation becoming initially more stable as  $E_s$  decreases towards the critical value or increases to more supercritical values. Moreover, the stability analysis also predicts that increasing curvature has a rapid destabilizing effect, so we may expect the behaviour to become rapidly more unstable as  $E_s^*$  is approached.

Figure 5 shows results for cases where the simulation is initialized by placing the quasi-steady solution on the grid, corresponding to two different initial values of  $r_s$  (110 and 200). In these cases the initial perturbation caused by the startup error induces an oscillation of the shock pressure (see Sharpe & Falle 2000a). However, figure 5 shows that the oscillations are very quickly damped out and the solution rapidly returns to being quasi-steady, showing that the underlying quasi-steady solution is highly stable away from the critical radius for  $E = 20$ , in agreement with the linear stability analysis.

## 5.2. $E = 24$

For  $E = 24$  the planar wave is stable, but now the neutrally stable radius of curvature predicted by the leading-order linear stability analysis (Watt & Sharpe 2003) is  $r_s/j = 403$ .

Figure 6(a) shows the shock pressure against shock radius in cylindrical geometry for  $E_s = 1300$ , which is near the critical initiation energy for  $E = 24$ , so that there is initially a large-amplitude ignition pulse in this case. By the time the overdrive of the detonation produced by this pulse has decayed back to near the quasi-steady speed, the curvature is not far from the neutrally stable value predicted by the linear analysis. Indeed, figure 6(a) shows that the amplitude of the oscillations is rather small and subsequently grows only slightly initially, before reaching a maximum and then decaying. Figures 6(b) and 6(c) show the results for slightly higher source energies ( $E_s = 1400$  and 1500, respectively).  $E_s = 1500$  is close to  $E_s^*$  for  $E = 24$  (i.e. that corresponding to the minimum radius of formation of the detonation). Note that the distinction between the ignition pulse and the instability becomes much less clear as  $E_s$  increases. However, ignoring this first pulse, the amplitude of the initial oscillations is largest for  $E_s = 1500$ . In both cases, the amplitude subsequently decreases.

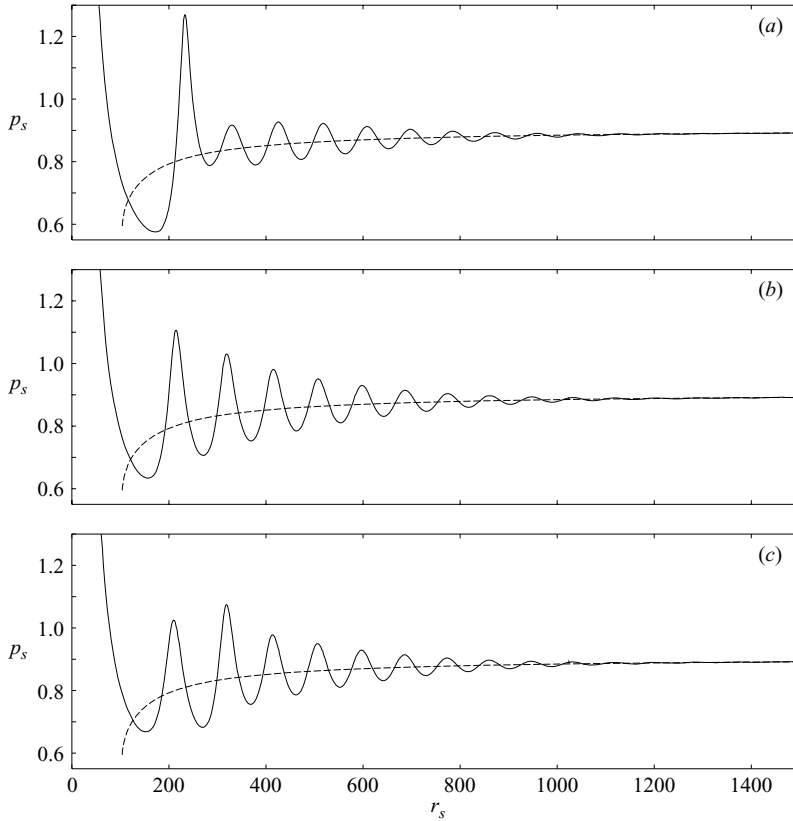


FIGURE 6. Shock pressure versus shock radius in cylindrical geometry for  $E = 24$  and (a)  $E_s = 1300$ , (b)  $E_s = 1400$  and (c)  $E_s = 1500$ . The dashed curve is the quasi-steady  $p_s-r_s$  relation.

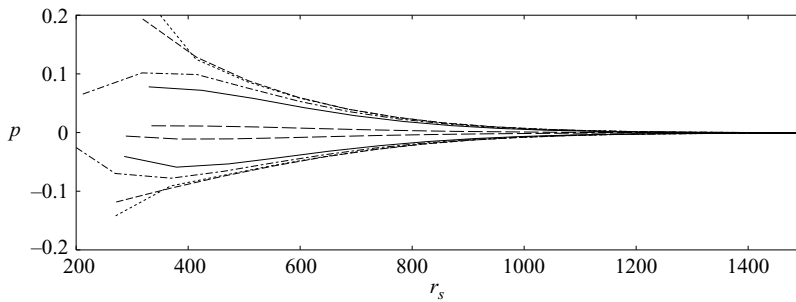


FIGURE 7. Oscillation amplitude envelopes for  $E = 24$  and  $E_s = 1300$  (solid lines), 1400 (dotted lines), 1500 (short-dashed lines), 2000 (dot-dashed lines) and 3000 (long-dashed lines).

Figure 7 shows the amplitude envelopes of the oscillations for each of the above source energies. Note that here we have first subtracted the quasi-steady  $p_s-r_s$  relation from the numerical data. Since the shock pressure oscillates around the quasi-steady value (which itself increases with shock radius), subtracting the quasi-steady pressure gives a much clearer picture of the growth and decay of the amplitudes (and hence where the maximum amplitudes occur). Note from figure 7 that, after the first couple

of pulsations, the amplitude envelopes for  $E_s = 1400$  and  $1500$  are virtually the same. It thus appears that for these source energies the oscillations quickly reach a saturated nonlinear amplitude, and subsequently the amplitude for these cases follows a ‘saturated nonlinear envelope’. This type of behaviour is much clearer for the  $E = 25$  case discussed in §5.3 below. For  $E_s = 1300$ , however, after the ignition pulse, the amplitude envelope of the pulsations lies completely within those of  $E_s = 1400$  and  $1500$ . Indeed, for this case figure 7 shows that the amplitude reaches a maximum somewhat before  $r_s = 400$  (cf. the linear neutral stability value of  $r_s = 403$ ) and then subsequently decays. For  $E_s = 1300$  it thus appears that the wave reaches a stability boundary before the amplitude reaches the saturated nonlinear envelope. Again, this type of behaviour is made much clearer in §5.3 below.

Figure 8 shows the shock pressure against shock radius for supercritical source energies when  $E = 24$  in cylindrical geometry. The amplitude envelopes for two of these cases are also shown in figure 7. Note that for these supercritical cases the detonation forms at a higher radius as  $E_s$  increases, and figure 8 shows that as it increases, both the initial amplitude of the oscillations and the growth rate of the amplitude decrease, in agreement with the linear stability prediction that decreasing curvature stabilizes the wave. Figure 7 shows that for both  $E_s = 2000$  and  $3000$ , the amplitude reaches a maximum (this maximum value decreases as  $E_s$  increases) around  $r_s = 400$  before decaying, indicating that a stability boundary has been crossed. For a sufficiently high source energy and hence sufficiently large radius at which the detonation forms, there is no initial growth of the oscillation amplitude (e.g. figure 8(d) for  $E_s = 5000$ ) showing that the quasi-steady detonation is stable at the radius at which it forms. Figure 8 shows that this critical radius of curvature above which the wave is stable from the outset is in good agreement with the linear neutral stability boundary of  $r_s = 403$ . Figure 9 shows the shock pressure histories from simulations which were initialized using the quasi-steady solution corresponding to  $r_s = 150$  and  $410$ . The results are qualitatively very similar to the directly initiated cases. Figure 10 shows the amplitude envelopes for these cases as well as that for a case with an initial shock radius of  $200$ . For  $r_s = 150$  and  $200$ , the amplitudes again reach maxima around  $r_s = 400$  before decaying, while for the  $r_s = 410$  case the amplitude decreases from the outset showing that the quasi-steady solution is stable for this initial shock radius. Note also that, as in the directly initiated cases, the smaller the initial radius, the more rapidly the initial oscillation amplitude grows. Again, these results are all in very good agreement with the linear stability predictions.

We now look briefly at spherical geometry. The main difference between cylindrical and spherical expanding detonations is that the underlying quasi-steady wave speed and structure, and their linear stability, are dependent on shock radius though the parameter  $r_s/j$ . Hence the shock radius corresponding to a given quasi-steady detonation speed (and corresponding linear growth rate) for a spherically expanding wave is twice that for a cylindrically expanding wave. For example, in spherical geometry, the linear stability analysis predicts that the neutrally stable radius is  $r_s = 806$  for  $E = 24$ . Hence the detonation wave is stabilized more slowly with increasing  $r_s$  in spherical geometry.

Figure 11 shows the shock pressure against shock radius for the spherical case, with  $E_s = 7000, 8000, 9000$  and  $10000$ . For  $E_s = 7000$  (a source energy which is near the critical value) and  $E_s = 10000$  (figures 11(a) and 11(d), respectively), the evolution looks qualitatively similar to some of the cases described for cylindrical geometry. However, the amplitude decreases more slowly in the spherical case, as expected from the stability analysis. After the first couple of oscillations, the amplitude envelopes

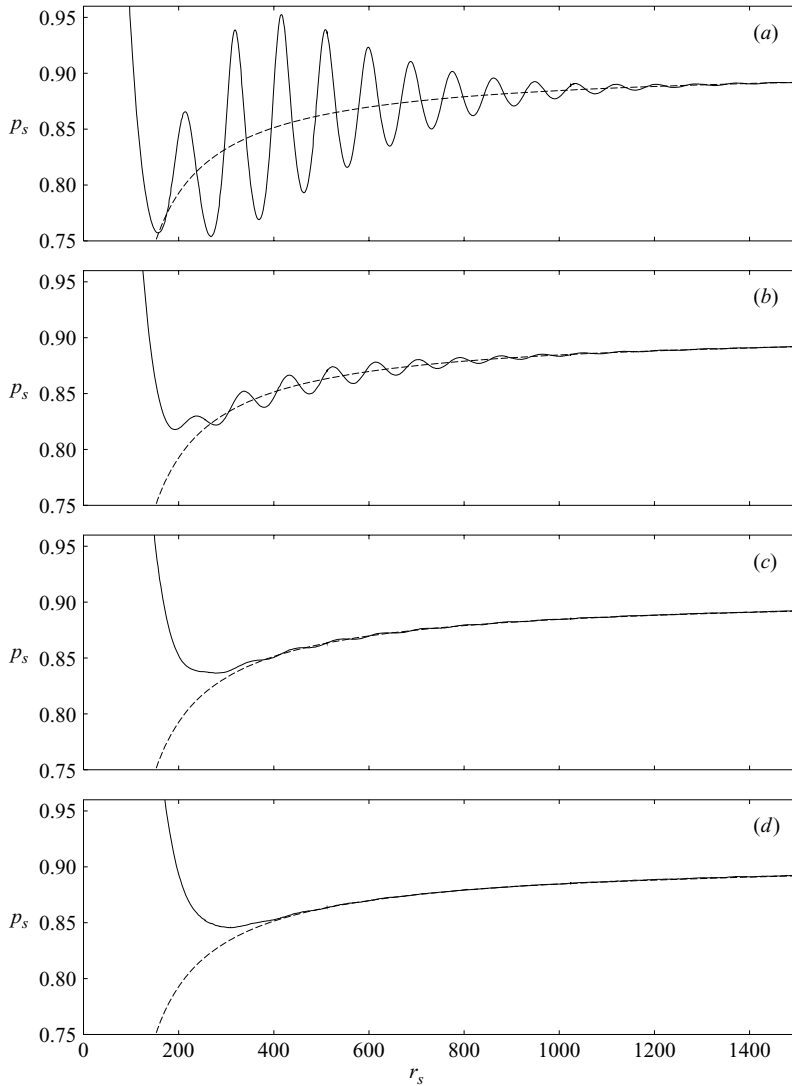


FIGURE 8. Shock pressure versus shock radius in cylindrical geometry for  $E = 24$  and (a)  $E_s = 2000$ , (b)  $E_s = 3000$ , (c)  $E_s = 4000$  and (d)  $E_s = 5000$ . The dashed curve is the quasi-steady  $p_s$ - $r_s$  relation.

of these two cases are identical, indicating that again they have reached a saturated nonlinear behaviour.

For  $E_s = 8000$  (a value close to that corresponding to the minimum radius of formation,  $E_s^*$ ) and  $E_s = 9000$  (figures 11(b) and 11(c), respectively), we see a different behaviour than for any case in cylindrical geometry. In these cases, there is initially an ignition pulse, but because the stability of the wave changes more slowly in spherical geometry, when the shock pressure subsequently approaches the quasi-steady state again, the shock curvature is still quite high compared to that after the ignition pulse in the cylindrical case. Indeed, for these source energies and spherically expanding waves, the curvature after the first pulse is still sufficiently high that the underlying quasi-steady wave is highly unstable here, and subsequently there is a large-amplitude

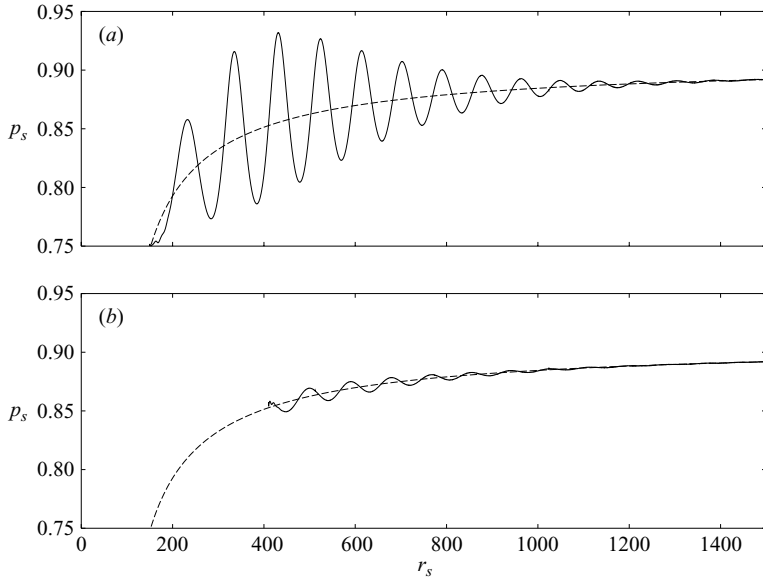


FIGURE 9. Shock pressure versus shock radius in cylindrical geometry for  $E = 24$  when the simulations are initialized by the quasi-steady solutions corresponding to (a)  $r_s = 150$  and (b)  $r_s = 410$ . The dashed curve is the quasi-steady  $p_s$ - $r_s$  relation.

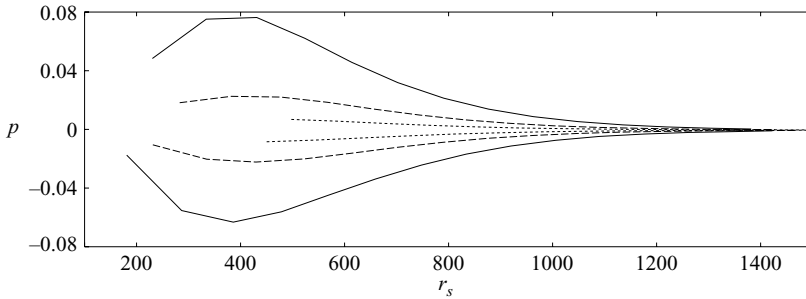


FIGURE 10. Oscillation amplitude envelopes for  $E = 24$  when the simulations are initialized by the quasi-steady solutions corresponding to  $r_s = 150$  (solid lines), 200 (dashed lines) and 410 (dotted lines).

oscillation, much like the type of oscillations seen in highly unstable cases in planar geometry (Sharpe & Falle 2000a). By the time the shock pressure again approaches the quasi-steady speed after this large-amplitude oscillation, the curvature is much smaller, and now we again see much lower-amplitude oscillations which at first grow in amplitude, pass through a maximum and then decay. The maximum amplitude in this final stage for  $E_s = 8000$  and  $E_s = 9000$  occurs at about  $r_s = 750$ , in reasonable agreement with the leading-order linear stability prediction of  $r_s = 806$ . Note that for these cases the second pulse itself acts like an ignition pulse, with the main evolution stage starting after this second pulse. In this main stage the oscillations begin with relatively small amplitude due to the shock pressure returning to near the quasi-steady values at relatively high  $r_s$  after the second peak. For the  $E_s = 10000$  case, however, the main evolution starts with the now smaller second peak, i.e. at a relatively small value of  $r_s$ . Hence the subsequent oscillations are larger in this case than for the

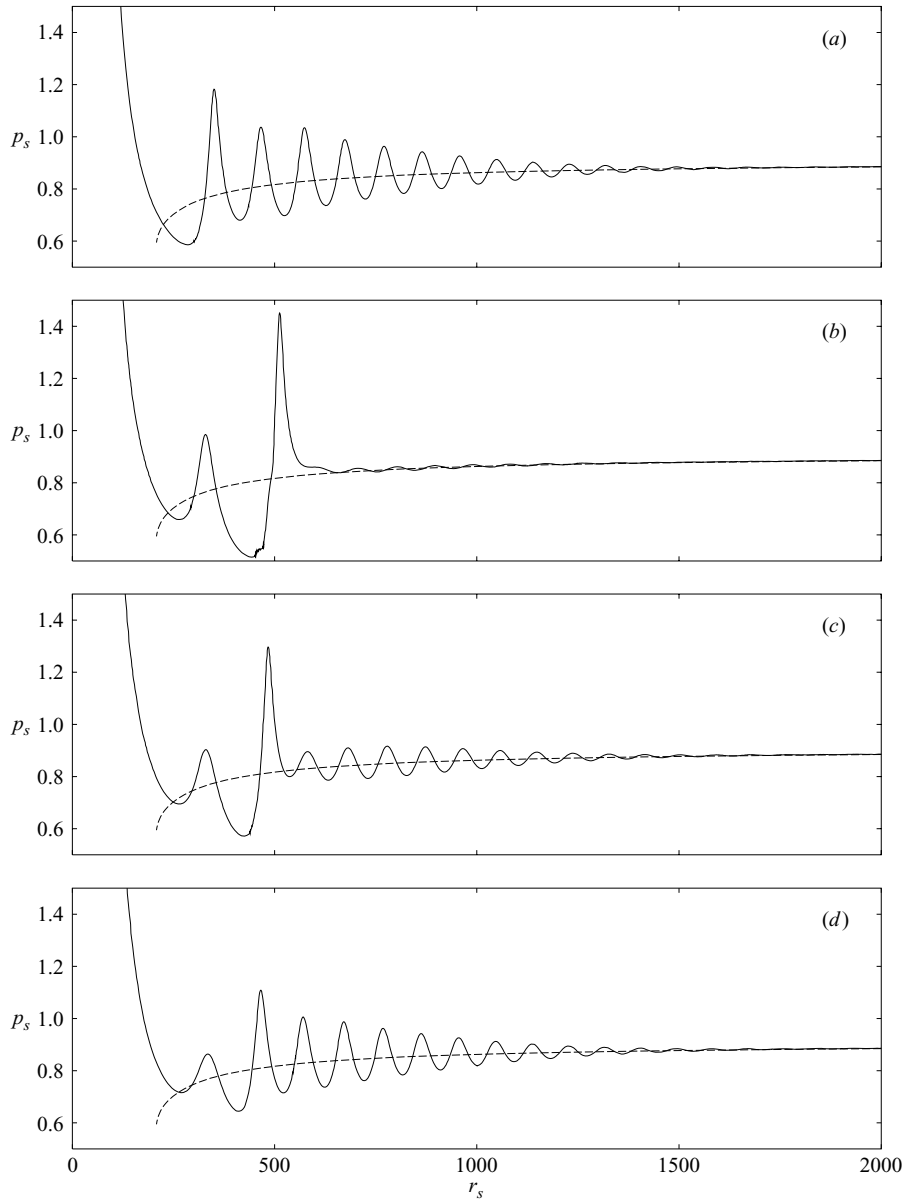


FIGURE 11. Shock pressure versus shock radius in spherical geometry for  $E = 24$  and (a)  $E_s = 7000$ , (b)  $E_s = 8000$ , (c)  $E_s = 9000$  and (d)  $E_s = 10000$ . The dashed curve is the quasi-steady  $p_s$ - $r_s$  relation.

higher  $E_s$  cases. Apart from the slower change of stability, the main conclusions of the paper are the same for spherical geometry as for cylindrical geometry, and hence we will not consider the spherical case further.

The main point of this section is that the above results from these nonlinear calculations confirm the predictions of the linear stability analysis in Watt & Sharpe (2003) that increasing curvature has a rapidly destabilizing effect on detonation waves. Furthermore, the stability boundary where the maximum oscillation amplitudes

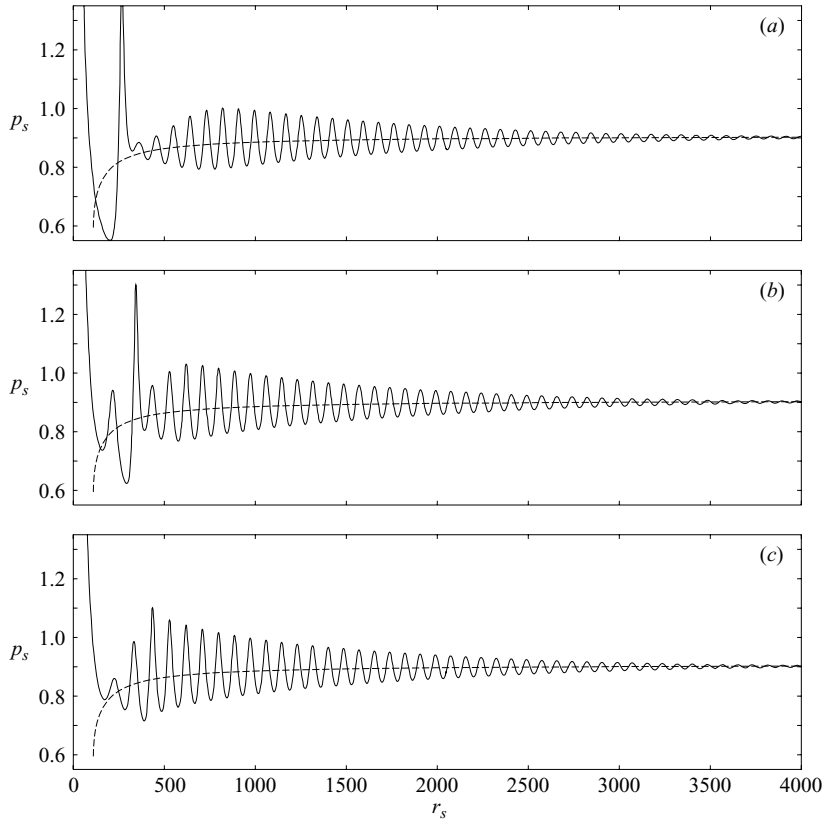


FIGURE 12. Shock pressure versus shock radius in cylindrical geometry for  $E = 25$  and (a)  $E_s = 1500$ , (b)  $E_s = 2000$  and (c)  $E_s = 2500$ . The dashed curve is the quasi-steady  $p_s$ - $r_s$  relation.

occurs, in cases where the shock reaches this boundary before the amplitude saturates, is in good agreement with the prediction of the stability boundary from the linear analysis. Similarly the critical radius of formation above which no oscillations are ever seen is also in good agreement with this neutral stability boundary.

### 5.3. $E = 25$

For an activation temperature of  $E = 25$ , the planar wave is still stable, but very near the neutrally stable value of  $E = 25.26$  (Sharpe 1997). The linear stability analysis in Watt & Sharpe (2003) predicts that the quasi-steady detonation will only be stable for radii of curvature above  $r_s = 1933$ .

Figure 12 shows the shock pressure evolution for source energies of  $E_s = 1500$ , 2000 and 2500. The value  $E_s = 1500$  (figure 12a) is near the critical initiation energy for  $E = 25$ . For this case there is initially a large-amplitude ignition pulse. By the time the speed of the overdriven detonation produced by this ignition event has dropped back to near the quasi-steady value, the shock curvature has become much smaller, so that the initial amplitude of the subsequent oscillations is relatively small, having a rather slow growth rate. The amplitude of these subsequent oscillations reaches a maximum and then decays. Figure 12(b) shows the results for the case  $E_s = 2000$ . This initiation energy is close to that corresponding to the value for which the radius of detonation formation is a minimum,  $E_s^*$ . In this case the first (ignition) pulse is

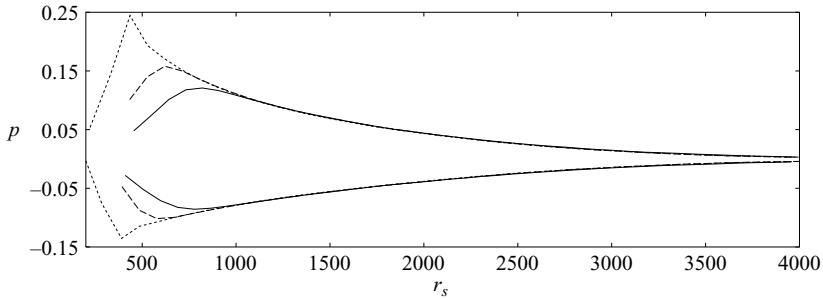


FIGURE 13. Oscillation amplitude envelopes for  $E = 25$  and  $E_s = 1500$  (solid lines), 2000 (dashed lines) and 2500 (dotted lines).

of much smaller amplitude than for  $E_s = 1500$ , but the radius of curvature after it is sufficiently small that the wave is still highly unstable. Hence in this case the shock pressure subsequently undergoes a large-amplitude pulse, similar to those which occur for very unstable detonations in the planar case (Sharpe & Falle 2000*a*). Again, by the time the shock speed has subsequently dropped back to near the quasi-steady value after this large-amplitude oscillation, the radius of curvature is rather high. The underlying quasi-steady detonation is thus now much less unstable, and so the amplitude of the subsequent oscillations and their growth rate is relatively small. The amplitude of these subsequent oscillations passes through a maximum after a couple of periods. Figure 12(*c*) shows the case of a more supercritical initiation energy of  $E_s = 2500$ . Now the amplitude of the oscillations initially grows monotonically, before reaching a maximum and decaying.

Figure 13 shows the amplitude envelopes for the three initiation energies used above. The main point to note is that (subsequent to any large-amplitude oscillations) once the oscillation amplitude reaches a maximum in each of these cases, its evolution is independent of the initiation energy. Hence for this activation temperature, there is now more clearly a ‘saturated nonlinear envelope’. It thus appears that for any given value of  $r_s$  there is an amplitude corresponding to the saturated nonlinear behaviour for that radius. From figure 13 it can be seen that the saturated amplitude increases rapidly with decreasing  $r_s$  as the quasi-steady critical radius is approached, since the detonation rapidly becomes more unstable here (cf. Sharpe & Falle 2000*a* for the planar case, where the amplitude of the final saturated oscillations increases as the activation temperature is increased). Note that (subsequent to any large-amplitude oscillations), there are two stages in the evolution: an initial stage of growth of the amplitude of the oscillation towards the saturated nonlinear envelope, followed by a stage in which the amplitude saturates and subsequently follows the envelope. The amplitude is hence a maximum when it just reaches the saturated envelope. Where this maximum occurs depends on the prior growth rate, which itself depends on the radius at which the growth stage begins (the smaller the radius the more unstable the detonation and hence the more rapid the growth).

Note that there is no evidence of the linear neutral stability boundary, predicted to be at  $r_s = 1933$ , in these cases. This is due to the fact that the oscillations have already reached the saturated nonlinear behaviour long before this stability boundary is reached, and hence the linear stability analysis is no longer valid.

Figure 14 shows the shock pressure evolution for various supercritical initiation energies, while figure 15 shows the corresponding amplitude envelopes. As for the case  $E_s = 2500$  above, for these supercritical source energies the amplitude initially

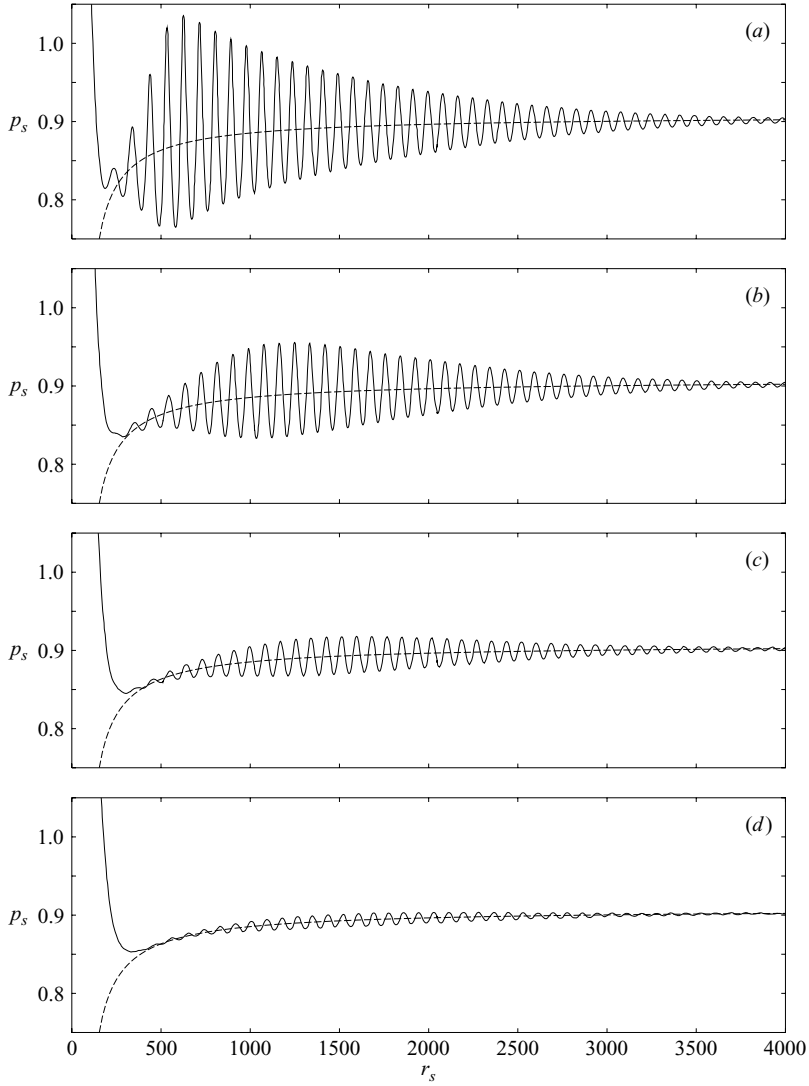


FIGURE 14. Shock pressure versus shock radius in cylindrical geometry for  $E = 25$  and (a)  $E_s = 3000$ , (b)  $E_s = 4000$ , (c)  $E_s = 5000$  and (d)  $E_s = 6000$ . The dashed curve is the quasi-steady  $p_s$ - $r_s$  relation.

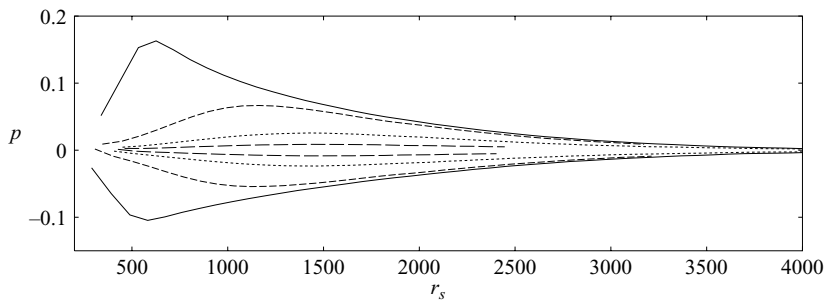


FIGURE 15. Oscillation amplitude envelopes for  $E = 25$  and  $E_s = 3000$  (solid lines), 4000 (short-dashed lines), 5000 (dotted lines) and 6000 (long-dashed lines).

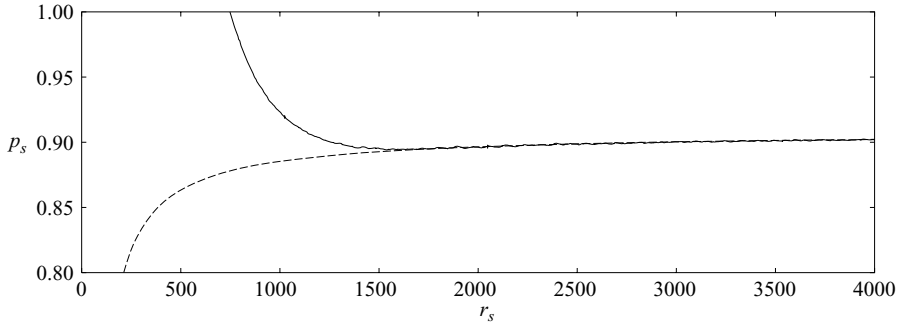


FIGURE 16. Shock pressure versus shock radius in cylindrical geometry for  $E = 25$  and  $E_s = 80000$ . The dashed curve is the quasi-steady  $p_s$ - $r_s$  relation.

grows monotonically. However, the initial amplitude and subsequent growth rate are smaller the more supercritical the initiation energy is. This is because the radius where the detonation first forms increases and hence the detonation is more stable from the outset. For  $E = 3000$  (figure 14a), the amplitude again reaches the saturated nonlinear envelope after a few periods. For the higher values of  $E_s$  however, figure 15 shows that the amplitude of the oscillations passes through a maximum before they reach the saturated envelope. Hence the amplitude envelopes for the higher  $E_s$  lie entirely within those for lower initiation energies. For these cases the growth of the oscillations is sufficiently slow that the wave reaches a nonlinear stability boundary before the amplitude saturates, and then subsequently decays. Since the growth rate is slower the higher the initiation energy, the amplitude reached before the stability boundary decreases. The value of  $r_s$  where this nonlinear stability boundary occurs (i.e. where the amplitude is a maximum) depends to some extent on the size of the amplitude, but as the amplitude here decreases (and hence the linear approximation becomes more valid), it tends to about  $r_s = 1500$ . Similarly, the critical radius of formation above which no oscillations are seen is also about  $r_s = 1500$  (see figure 16 for  $E_s = 80000$ ).

However, the quasi-steady initialized simulations give much better agreement with the linear stability boundary prediction of  $r_s = 1933$ . Figure 17 shows the results for a couple of quasi-steady-solution initialized cases, while figure 18 shows the amplitude envelopes corresponding to several different initial shock radii. For these cases, figure 18 shows that the position of the maximum amplitude is around 1600 for the most unstable cases shown (corresponding to an initial shock radius of 500), but that the position of the maximum amplitude increases with increasing initial shock radius, and tends towards around  $r_s = 1900$ , in good agreement with the linear prediction. For the case with an initial radius  $r_s = 2000$ , the amplitude monotonically decreases, showing that the quasi-steady solution is stable at this radius.

The reason why the stability boundary of  $r_s \sim 1500$  in the directly initiated cases does not agree quantitatively with the linear analysis for this case is explained by figure 19. For this activation temperature, the stability boundary occurs at quite a large  $r_s$ . It can be seen from the shock pressure evolution figures that at such high radii the underlying quasi-steady shock pressure (and speed and structure) is very slowly varying with  $r_s$ . For example at  $r_s = 1500$ ,  $p_s = 0.893$  for the quasi-steady wave, while the shock pressure is only slightly larger,  $p_s = 0.896$ , at  $r_s = 1933$ . Similarly, the linear stability response of the quasi-steady wave will also be insensitive to  $r_s$  at these larger radii. Indeed, figure 19 shows the leading-order linear growth rate for

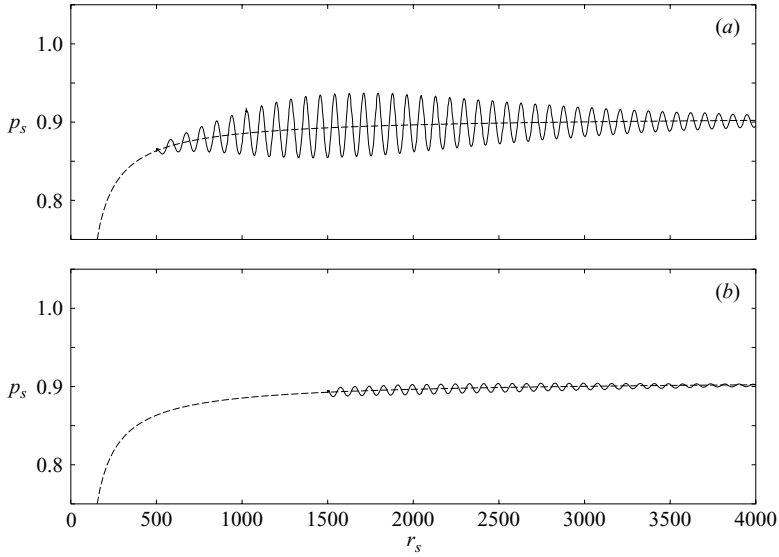


FIGURE 17. Shock pressure versus shock radius in cylindrical geometry when the simulations are initiated by the quasi-steady solutions corresponding to (a)  $r_s = 500$  and (b)  $r_s = 1500$ . The dashed curve is the quasi-steady  $p_s$ - $r_s$  relation.

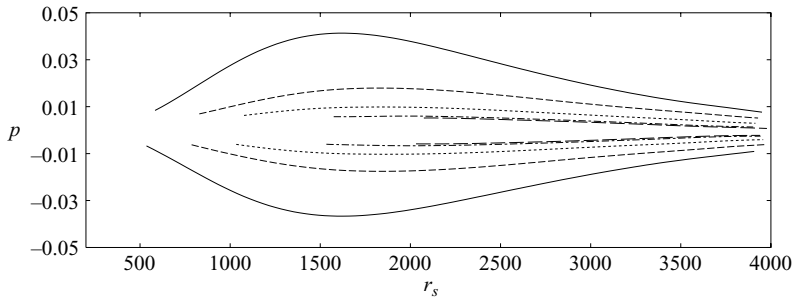


FIGURE 18. Oscillation amplitude envelopes when the simulations are initialized by the quasi-steady solutions corresponding to  $r_s = 500$  (solid lines), 750 (short-dashed lines), 1000 (dotted lines), 1500 (dot-dashed lines) and 2000 (long-dashed lines).

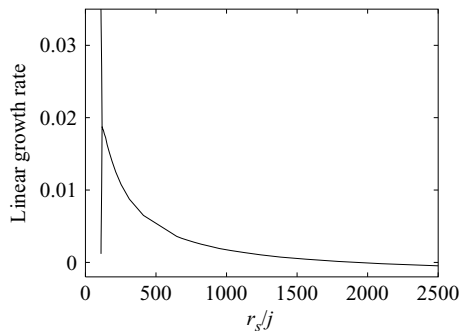


FIGURE 19. Leading order linear growth rate versus  $r_s/j$  for  $E = 25$ .

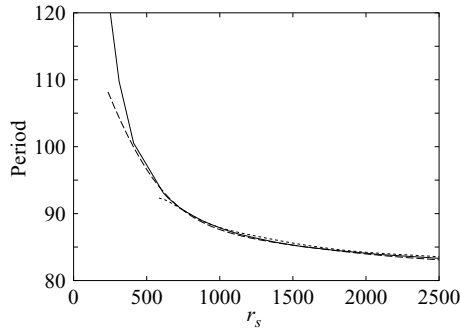


FIGURE 20. Periods of oscillation versus  $r_s$  for  $E = 25$  in cylindrical geometry. Leading-order linear period (solid line) and periods from directly initiated simulation with  $E_s = 3000$  (dashed line) and from quasi-steady solution initialized simulation with initial  $r_s = 500$  (dotted line).

$E = 25$  against  $r_s$ , from which it can be seen that the growth rate varies only weakly with  $r_s$  for shock radii greater than about 1000 (as  $r_s$  decreases and the curvature of the front begins to increase rapidly, the growth rate begins to accelerate, and then splits into two real eigenvalues as the critical quasi-steady curvature is approached). Since the magnitude of the growth rate remains very small at these high radii, any small residual time-dependence in the underlying wave in the directly initiated cases or any weak nonlinearity in the oscillations may shift the actual stability boundary by a relatively large value of  $r_s$  from the leading-order quasi-steady prediction. Nevertheless, the leading-order analysis still provides a qualitatively good prediction of the boundary even for the directly initiated case, and more importantly provides the correct parametric dependency of its location. Furthermore, the analysis does provide a quantitatively good prediction of the neutrally stable quasi-steady shock pressure (or speed).

For the planar case, near the stability boundary the linear period of oscillation predicts well the period of the oscillations, even when they have reached the saturated nonlinear (limit cycle) amplitude (Sharpe & Falle 2000a; Short & Quirk 1997). Hence one may expect that for the expanding detonation case, the linear dependence of the period on  $r_s$  may predict well the change in the period of the oscillations as the front expands outwards. Figure 20 shows the linear dependence of the period on  $r_s$  and also the periods from the numerical simulations (defined as the distance between adjacent crests in the oscillation amplitude) for both a directly initiated case and a quasi-steady-solution initialized case. Importantly, note that for the directly initiated case (corresponding to  $E_s = 3000$ ), the oscillations quickly reach the saturated nonlinear envelope. It can be seen that the linear stability analysis predicts extremely well the periods in the simulations, even in the saturated nonlinear regime. Note that the period is long compared to the particle transit time through the quasi-steady wave, but short on the slow evolution timescale of the quasi-steady solution.

#### 5.4. $E = 27$

For  $E = 27$ , the planar wave is unstable, and hence in this case the oscillations will always eventually reach a saturated behaviour, regardless of  $E_s$ , as there is no stability boundary. In the planar case, this activation temperature is just below a period-doubling bifurcation boundary (at  $E = 27.2$ ) (Sharpe & Falle 2000a). We may thus expect that even at quite large radii of curvatures for  $E = 27$ , the increase in instability will cause the saturated nonlinear behaviour to period double, with the behaviour

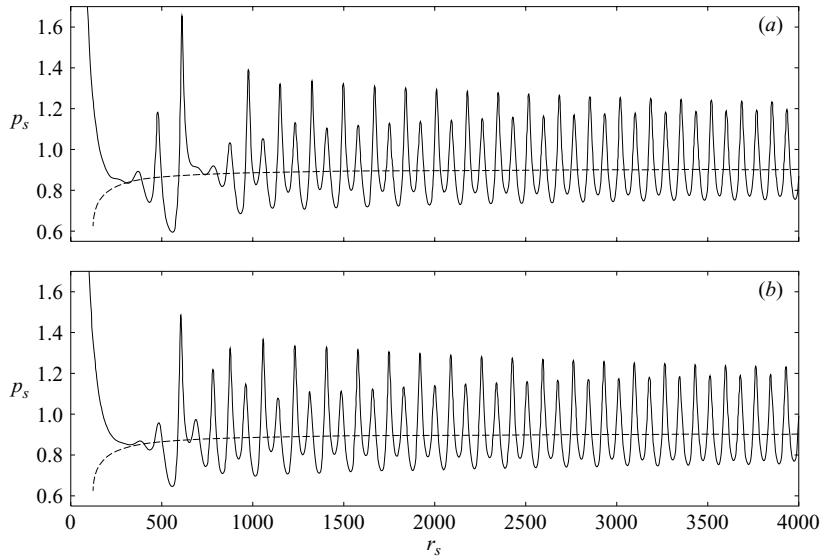


FIGURE 21. Shock pressure versus shock radius in cylindrical geometry for  $E = 27$  and (a)  $E_s = 5000$ , (b)  $E_s = 6000$ . The dashed curve is the quasi-steady  $p_s$ - $r_s$  relation.

tending to that of the limit cycle in the planar case considered in Sharpe & Falle (2000a) only at very large  $r_s$ . This is exactly what is seen in figure 21, which shows the shock pressure evolution for two source energies,  $E_s = 5000$  and  $6000$ . In both cases, the detonation forms at a shock radius which is sufficiently small for the detonation to be highly unstable in this case, which results in a large-amplitude oscillation associated with such unstable waves (Sharpe & Falle 2000a). Once the shock pressure drops back towards the quasi-steady values after this large-amplitude oscillation, the radius is much higher and hence the detonation is less unstable. Subsequently, however, a saturated nonlinear behaviour is quickly reached. It appears in both cases that the saturated behaviour of the first few oscillations of this stage are actually that of a 4-period oscillation. The oscillations then bifurcate to a period-doubled behaviour, but the difference between the high- and low-amplitude oscillations decreases as the front expands towards less unstable radii, so that the behaviour is tending to that of limit-cycle-type oscillations at large  $r_s$ , as expected. Again, these results show that curvature has a rapid destabilizing effect on detonation waves. Note that the amplitude envelopes of both the high- and low-amplitude oscillations are identical for both source energies during the period-doubled oscillation stage.

Short & Quirk (1997) and Radulescu *et al.* (2002) have shown that, in the planar case for realistic chemistry models, detonations have a definite one-dimensional detonability limit due to the pulsating instability. They showed that as a stability parameter is varied such that the wave becomes more unstable, eventually the amplitude of the pulsation becomes so large as to drive the shock temperature too low to initiate the exothermic chemical reactions and the detonation subsequently fails. Hence for values of the stability parameters beyond this point the detonation cannot propagate in one dimension.

In our case the curvature is the main stability parameter. Hence if the planar wave is sufficiently unstable (i.e. for high enough  $E$ ), we may expect that a shock radius corresponding to a one-dimensional failure limit exists. For radii below this limit radius the underlying quasi-steady wave becomes sufficiently unstable that the

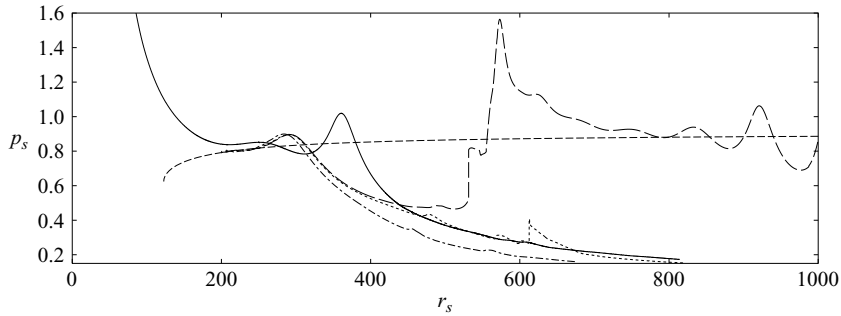


FIGURE 22. Shock pressure versus shock radius in cylindrical geometry for  $E = 27$  when the simulations are initialized with the quasi-steady solution corresponding to  $r_s = 200$  (dot-dashed line), 206 (dotted line) and 207 (long-dashed line). Also shown is the directly initiated solution for  $E_s = 4000$  (solid line). The short-dashed curve is the quasi-steady  $p_s$ - $r_s$  relation.

pulsations drive the shock temperature too low for continued propagation of the front. This is confirmed by figure 22 in which the results for cases where the simulations were initialized by the quasi-steady solutions for various initial values of  $r_s$  are shown. Figure 22 reveals that in this case the limit value of  $r_s$  is 206, below which the detonation quickly fails, and above which the detonation manages to keep propagating (note the failure limit would be more sharply defined for realistic chemistry models). Note that as  $E$  increases and the planar wave becomes more unstable, a smaller increase in curvature will be required for the wave to become unstable enough to fail, and hence the limit radius will move towards higher  $r_s$ .

The presence of this failure-limit radius suggests that even for ‘supercritical’ source energies where the blast wave approaches the quasi-steady curve above the critical quasi-steady radius but below the limit radius, the detonation will fail to be initiated in one dimension since even if it initially forms from the decaying blast wave, it will subsequently fail again due to the instability. Again, this is confirmed in figure 22 which also shows the result for a directly initiated case with  $E_s = 4000$ .

Indeed, Eckett *et al.* (2000) found that for a case they considered, successful detonation initiation did not depend monotonically on  $E_s$ . They showed that initially as the source energy was increased above the minimum critical source energy, a detonation was successfully initiated, but then for a range of higher values of  $E_s$ , the detonation failed subsequently to initiation. For all source energies above this range of  $E_s$ , a detonation was again successfully initiated. This behaviour in Eckett *et al.* (2000) is hence explained by the results of this section: for the case they considered there clearly exists a failure-limit shock radius associated with the instability. For sufficiently near critical or sufficiently supercritical source energy, the detonation forms above this failure-limit radius, and hence continues to propagate after formation. However for a range of source energies close to  $E_s^*$  (the source energy corresponding to the minimum radius of detonation formation), the detonation forms below the failure radius and hence the instability quickly kills the wave after it has formed, leading to failure not only below the critical source energy but also for a range of  $E_s$  near  $E_s^*$ .

However, it is important to note that while the detonation fails in one dimension in these cases, it does not mean that in reality it will fail, but that multi-dimensional effects such as the cellular instability will play the crucial role in determining whether the wave can propagate or whether a detonation will be successfully initiated for source energies close to  $E_s^*$ .

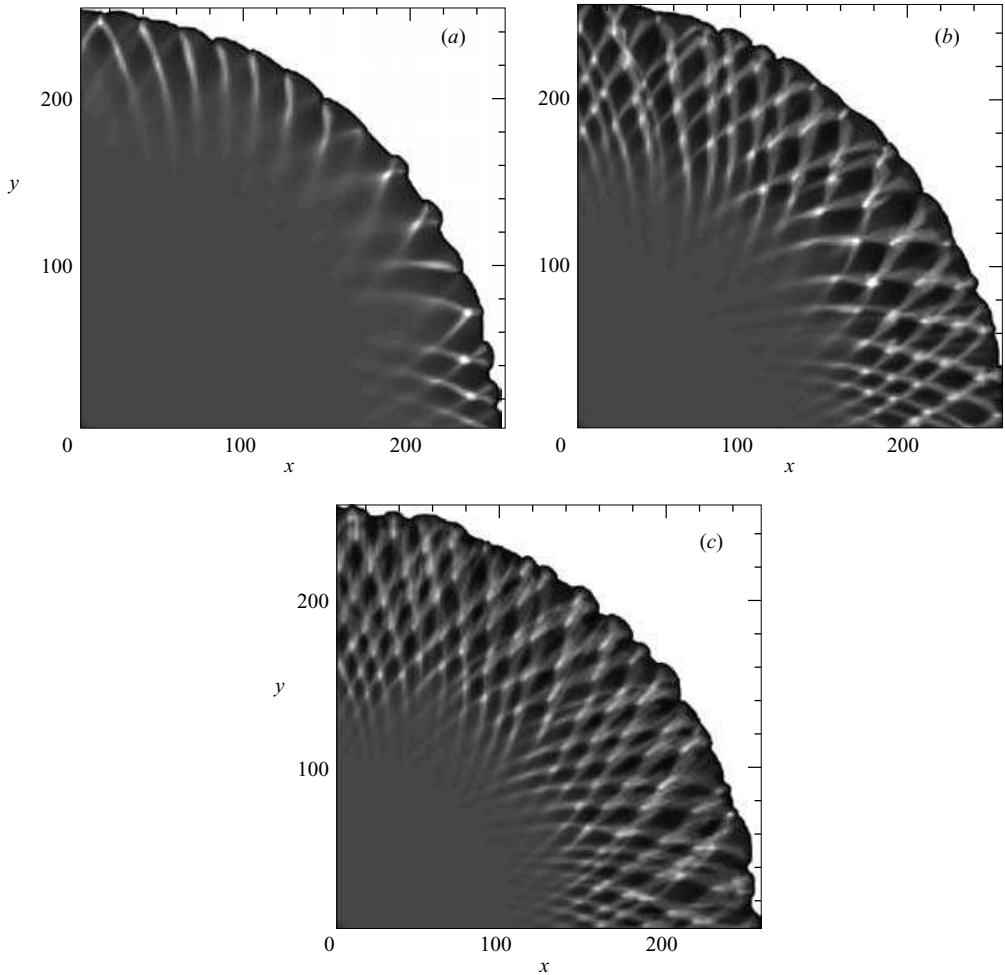


FIGURE 23. Detonation cells for  $E = 24$  and  $E_s = 3200$  and numerical resolutions of (a) 4, (b) 8 and (c) 16 points/ $l_{1/2}$ . The greyscale is the total heat released at each point for values ranging from 0 (black) to 3.5 (white).

## 6. Cellular instability

In multi-dimensionally unstable (or ‘cellular’) detonations, the shock front becomes wrinkled and kinked, and is joined at triple points by transverse shock waves which extend back into the reaction zone. These transverse waves collide with each other and hence travel back and forth in the direction transverse to the front. The paths of the triple points make diamond-shape patterns as the transverse waves continually collide and reflect (Fickett & Davis 1979). Note that, while gaseous detonations are only unstable to the pulsating instability provided the state sensitivity of the reaction rate is sufficiently high, they are always unstable to the cellular instability (unless both the heat release and activation temperature are unrealistically small) (Short & Stewart 1998).

In order to determine the effects of curvature on the cellular instability for expanding detonation waves, one could attempt to perform two-dimensional numerical simulations. Figure 23 shows the results for  $E = 24$  and  $E_s = 3200$ , using numerical

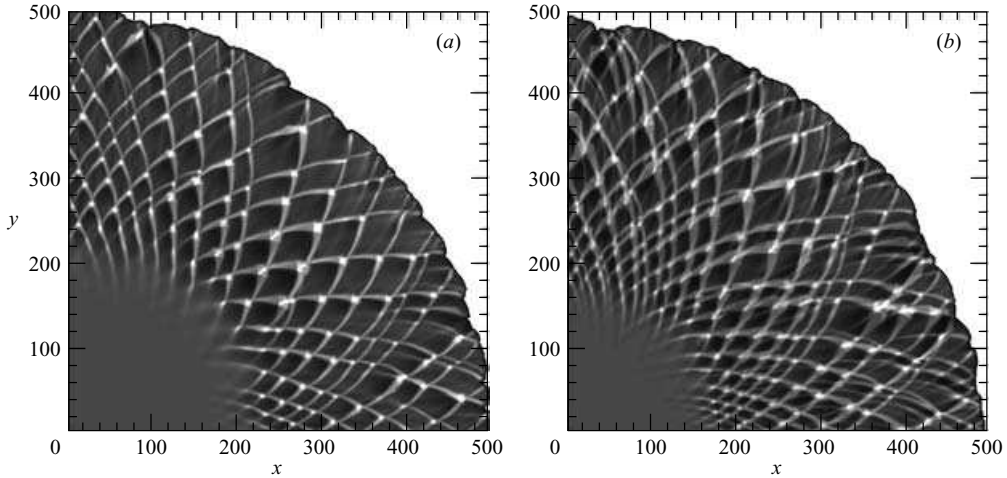


FIGURE 24. As figure 23 (*a*, *b*) but showing the cellular evolutions after a longer time.

resolutions of 4, 8 and 16 points/ $l_{1/2}$ . The figure shows greyscale plots of the total heat released at each point in the numerical domain (see Sharpe & Falle 2000*c*). The main point to note is that at these resolutions, the cell sizes and evolution are completely grid-dependent. The cells appear only once the decaying blast wave has approached the quasi-steady detonation speed, i.e. when the reactions become important to sustaining the shock, as expected. However, the cells appear earlier with a smaller size as the resolution increases (presumably tending to the size corresponding to the wavelength with the maximum linear growth rate at the shock radius where they form, as in Sharpe & Falle 2000*c* for the planar case). The size of the cells also appears to grow more slowly as the resolution increases. Figure 24 shows the cellular evolutions after a longer time for the 4 and 8 points/ $l_{1/2}$  resolution cases. At the lower resolution, the cells grow but remain quite regular, while for the 8 points/ $l_{1/2}$  case, the cells are much more irregular and one can see weak tracks appearing as new triple points are generated as the front expands.

Hence, in order to obtain correct, grid-independent results from such simulations, much higher resolutions than those used in figures 23 and 24 are required. Simulations of cellular detonations in tubes show that at least about 50 points/ $l_{1/2}$  are required to ensure that all the lengthscales involved in the instability are resolved (Sharpe & Falle 2000*c*; Sharpe 2001). However, for the cylindrically expanding case in two dimensions, such requisite high resolutions are computationally prohibitive. This is due to the fact that while large numbers of points in the reaction zone are required, the shock front circumference is large on the reaction-zone scale, even when the detonation (and the cells) first form and even for the quarter-plane as considered here. This results in a very high number of grid points over the entire detonation front. As the wave front expands outwards, the length of the front increases, and hence so does the computational cost. Note that halving the grid size (i.e. doubling the number of points/ $l_{1/2}$ ) increases the computational time by a factor of 8 (double the number of grid points in each direction, and double the number of timesteps for a fixed Courant number). Note also that a uniform grid calculation with an equivalent resolution to that in our dynamically adaptive grid calculations would take more than an order of magnitude longer time, with this disparity increasing with the resolution.

To give an idea of the computational cost, even with an adaptive grid scheme, the calculation with 8 points/ $l_{1/2}$  in figure 24(b) (up to the point where  $r_s \approx 500$ ) took over 2 weeks of continuous run time on a dedicated 1.9 GHz processor, while the 16 points/ $l_{1/2}$  case, which ran up to the point where  $r_s \approx 260$  (figure 23c) took about 3 weeks on a similar dedicated processor. An equivalent run with a resolution of 64 points/ $l_{1/2}$ , or two additional refinement levels, would thus take about 3.7 years. Hence, to perform parametric studies (on  $E$  and  $E_s$  for example, as in §5) with a sufficiently high resolution to obtain reliable results ( $>50$  points/ $l_{1/2}$ ) would be almost impossible, even with an adaptive code and even on a parallel machine.

Nevertheless, the cellular instability will be crucial for determining whether the front can propagate in some cases, e.g. when the wave would fail in one dimension. Indeed, recent experiments in porous-walled tubes by Radulescu & Lee (2002) and Radulescu (2003) clearly show that for detonations with very regular cells, the cellular instability plays no crucial role in the propagation of the front. However, for highly unstable detonations with very irregular cells, they showed the presence of the transverse waves is in fact crucial for the wave to continue to propagate. Moreover, direct initiation experiments show that in some mixtures the wave fails if new transverse waves are not generated sufficiently rapidly to maintain a roughly constant spacing as the wave expands outwards (Lee 1977), and hence in these cases the cellular instability is the crucial factor for determining the successful initiation.

## 7. Conclusion

In this paper we have performed numerical simulations of cylindrically and spherically expanding detonations as a first step towards understanding the effect of curvature on the stability and propagation of detonations, and compared the nonlinear results with the recent linear stability analysis in Watt & Sharpe (2003).

First, one-dimensional numerical simulations of the pulsating detonation instability were performed. The main conclusion is that, in agreement with the linear analysis, increasing curvature of the front has a rapid destabilizing effect on detonation waves. The initial behaviour (e.g. amplitude and growth rate of pulsations) depends sensitively on the radius where the detonation first forms (i.e. on the source energy  $E_s$  for the directly initiated expanding waves). The closer the radius of formation is to the turning point of the quasi-steady  $p_s-r_s$  curve, the more unstable this behaviour. The radius is a minimum (and hence the detonation is initially most unstable) for a value of the source energy,  $E_s^*$ , which is above the critical source energy for successful initiation.

For cases where the planar wave (corresponding to infinite shock radius) is unstable, if the detonation is successfully initiated then the pulsations quickly reach a saturated nonlinear behaviour which is independent of the initial conditions. These saturated nonlinear oscillations tend to more stable behaviour as the front expands (e.g. it may pass backward through period-doubling bifurcations). However, for cases where the planar wave is one-dimensionally stable, there exists a neutrally stable shock radius above which the wave becomes stable. If the oscillations reach this boundary before they reach the saturated nonlinear state, then the amplitude subsequently decays. Alternatively, if the detonation initially forms above this radius, then no oscillations are seen and the wave propagates in a quasi-steady manner from the outset. The leading-order linear stability analysis in Watt & Sharpe (2003) provides a qualitatively good prediction of this neutrally stable shock radius, and a quantitatively good prediction of the neutrally stable quasi-steady detonation speed.

In future studies we intend to perform further analyses and simulations in order to get a better understanding of the effects of curvature on the detonation instabilities, and of the role of these instabilities in the propagation of curved fronts. First, since we have shown that the one-dimensional linear analysis correctly predicts the effect of curvature on detonations, we intend to perform a multi-dimensional analysis of cylindrically expanding fronts. Secondly, we intend to perform multi-dimensional numerical simulations of detonations where the front is curved but not expanding, so that the front is not too long compared to the reaction-zone length and hence sufficient resolution can be achieved. Such situations arise, for example, in weakly confined detonations, such as in condensed-phase explosives, and also gaseous detonations in porous-walled tubes.

This work was funded by EPSRC and DSTL under the Joint Grant Scheme. Cobra was supplied by Mantis Numerics Ltd.

## REFERENCES

- BOURLIOUX, A. & MAJDA, M. J. 1992 Theoretical and numerical structure for unstable two-dimensional detonations *Combust. Flame* **90**, 211–229.
- ECKETT, C. A., QUIRK, J. J. & SHEPHERD, J. E. 2000 The role of unsteadiness in direct initiation of gaseous detonations *J. Fluid Mech.* **421**, 147–183.
- ERPENBECK, J. J. 1964 Stability of idealized one-reaction detonations *Phys. Fluids* **7**, 684–696.
- FICKETT, W. & DAVIS, W. C. 1979 *Detonation*. University of California Press.
- HE, L. & CLAVIN, P. 1994 On the direct initiation of gaseous detonations by an energy source *J. Fluid Mech.* **277**, 227–248.
- LEE, J. H. S. 1977 Initiation of gaseous detonations *Annu. Rev. Phys. Chem.* **28**, 75–104.
- MAZAHARI, K. 1997 Mechanism of onset of detonation in blast initiation PhD Thesis, McGill University.
- NG, H. D. & LEE, J. H. S. 2003 Direct initiation of detonation with a multi-step reaction scheme *J. Fluid Mech.* **476**, 179–211.
- RADULESCU, M. I. 2003 The propagation and failure mechanism of gaseous detonations: experiments in porous-walled tubes PhD Thesis, McGill University.
- RADULESCU, M. I., HIGGINS, A. J., LEE, J. H. S. & MURRAY, S. B. 2000 On the explosion length invariance in direct initiation of detonation *Proc. Combust. Inst.* **28**, 637–644.
- RADULESCU, M. I., HIGGINS, A. J., MURRAY, S. B. & LEE, J. H. S. 2003 An experimental investigation of the direct initiation of cylindrical detonations *J. Fluid Mech.* **480**, 1–24.
- RADULESCU, M. I. & LEE, J. H. S. 2002 The failure mechanism of gaseous detonations: experiments in porous-walled tubes *Combust. Flame* **131**, 29–46.
- RADULESCU, M. I., NG, H. D., LEE, J. H. S. & VARATHARAJAN, B. 2002 The effect of argon dilution on the stability of acetylene-oxygen detonations *Proc. Combust. Inst.* **29**, 2825–2831.
- SHARPE, G. J. 1997 Linear stability of idealized detonations *Proc. R. Soc. Lond. A* **453**, 2603–2625.
- SHARPE, G. J. 2000 The structure of planar and curved detonation waves with reversible reactions *Phys. Fluids* **12**, 3007–3020.
- SHARPE, G. J. 2001 Transverse waves in numerical simulations of cellular detonations *J. Fluid Mech.* **447**, 31–51.
- SHARPE, G. J. & FALLE, S. A. E. G. 2000a Numerical simulations of pulsating detonations: I. Nonlinear stability of steady detonations *Combust. Theory Model.* **4**, 557–574.
- SHARPE, G. J. & FALLE, S. A. E. G. 2000b One-dimensional nonlinear stability of pathological detonations *J. Fluid Mech.* **414**, 339–366.
- SHARPE, G. J. & FALLE, S. A. E. G. 2000c Two-dimensional numerical simulations of idealized detonations *Proc. R. Soc. Lond. A* **456**, 2081–2100.
- SHORT, M. 2001 A nonlinear evolution equation for pulsating Chapman–Jouguet detonations with chain-branching kinetics *J. Fluid Mech.* **430**, 381–400.

- SHORT, M. & QUIRK, J. J. 1997 On the nonlinear stability and detonability limit of a detonation wave for a model three-step chain-branching reaction *J. Fluid Mech.* **339**, 89–119.
- SHORT, M. & SHARPE, G. J. 2003 Curved detonations for a two-step reaction. *Combust. Flame*, submitted.
- SHORT, M. & SHARPE, G. J. 2004 Failure and ignition limits of curved three-step chain-branching detonations *Combust. Theory Model.*, submitted.
- SHORT, M. & STEWART, D. S. 1998 Cellular detonation stability. Part 1. A normal-mode linear analysis *J. Fluid Mech.* **368**, 229–262.
- WATT, S. D. & SHARPE, G. J. 2003 One-dimensional linear stability of curved detonations *Proc. R. Soc. Lond. A* **460**, 2551–2568.
- YAO, J. & STEWART, D. S. 1996 On the dynamics of multi-dimensional detonation *J. Fluid Mech.* **309**, 225–275.